Computational Materials Science 57 (2012) 2–7

Contents lists available at ScienceDirect

Computational Materials Science

journal homepage: www.elsevier.com/locate/commatsci

A trans-scale model for size effects and intergranular fracture in nanocrystalline and ultra-fine polycrystalline metals

Bo Wu, Lihong Liang, Hansong Ma, Yueguang Wei *

LNM, Institute of Mechanics, Chinese Academy of Science, Beijing 100190, China

ARTICLE INFO

Article history:
Received 19 November 2010
Received in revised form 1 March 2011
Accepted 31 March 2011
Available online 21 April 2011

Keywords:
Interface energy effect
Strain gradient effect
Intergranular fracture
Nanocrystalline metal
Cohesive model

ABSTRACT

A trans-scale mechanics model considering both strain gradient and interface energy effects is presented for describing size effects in nanocrystalline and ultra-fine polycrystalline metals accompanying by intergranular fracture. A finite element method is developed which is suitable for describing the strain gradient and interface energy effects. Moreover, cohesive interface model is used to study the intergranular damage and fracture in polycrystalline metals with nanoscale and ultra-fine grains. A systematical study on the overall strength and ductility of polycrystalline aggregates which depend on both grain interiors and grain boundaries for different grain sizes and different interface properties is performed. The results show that the overall strength and ductility of polycrystalline aggregates with nanoscale and ultra-fine grains strongly depend on the grain size and grain hardening, interface energy density, grain boundary strength and toughness.

1. Introduction

Mechanical behaviors of polycrystalline materials with grain sizes typically less than 100 nm (nanocrystalline (nc) metals) or within 100–1000 nm (ultra-fine crystalline (ufc) metals) have undergone intensely worldwide attention over the past two decades. The nc/ufc metals exhibit the higher yield strength, tensile strength, and hardness, but the lower tensile ductility relative to bulk case. Although some micromechanisms have been presented for governing the mechanical behavior of polycrystalline aggregates [1–3], very few direct experimental evidences exist to show the fracture and failure processes in nc and ufc metals, especially inelastic deformation competition of grain interior and grain boundary. Shan et al. [4] reported that grain boundary–mediated processes of nc nickel film dominate its deformation through transmission electron microscope (TEM) observation. Moreover, many molecular dynamics (MD) simulations have shown that grain boundary related slip and separation phenomena plays an important role in the overall inelastic response of a polycrystalline materials with grain-size decrease [5–9]. Due to the limitations of time and dimensional scales in MD simulations for simulating the mechanical behaviors of the nc/ufc metals with realistic experiment sample sizes and strain rates, several continuum constitutive models have been used to describe the grain boundary effect and the failure response for the nc materials [3,10–16]. Studies using the high-resolution transmission electronic microscopy (HRTEM) have shown that the feature of intercrystalline grain boundary regions strongly depends on how the material is processed. Many grain boundaries appear sharp, well-defined and no distinct grain boundary phases, the others have shown considerable disorder in grain boundary regions [2,17]. Considering the inherently characteristic of grain boundaries in the nc/ufc metals, both the grain boundary affected zone (GBAZ) model [3,11–13] and the traction–separation cohesive interface model [14,15] were proposed to characterize the grain boundary response in polycrystalline aggregates.

Despite that the comprehensive computational analyses of mechanical behavior for the nc/ufc materials by using above mentioned continuum models were carried out recently, it is still difficult to unambiguously define the interfacial properties of grain boundaries. The conventional elastic–plastic theory is also impossible to characterize the size effects of mechanical behavior for the nc/ufc materials. In the present research, a trans-scale model considering both strain gradient effect and interface energy effect is presented for describing size effects of mechanical behavior for the nc/ufc metals accompanying by intergranular damage and fracture. A finite element method is developed which is suitable for describing both strain gradient effect and interface energy effect. Moreover, cohesive interface model is used to study the intergranular damage and fracture in polycrystalline metals with nanoscale and ultra-fine grains. Particular attention is focused on the influence of both grain interiors and grain boundary properties on the overall strength and ductility of the nc/ufc metals.

* Corresponding author.
E-mail address: Ywei@LNM.imech.ac.cn (Y. Wei).

0927-0256/$ - see front matter © 2011 Elsevier B.V. All rights reserved.
doi:10.1016/j.commatsci.2011.03.045

2. A trans-scale mechanics model for nano-structured materials

For the ufc metals (grain size is within the region: 100–10000 nm), in order to describe the size effects of mechanical behavior, one can use the strain gradient theory. However, for the nanocrystalline metals (nc, grain size is within the region: 10–1000 nm), besides the strain gradient effect, interface energy effect is also important. Therefore, it is necessary to develop a mechanics model to describe the size effects of mechanical behavior for the nanocrystalline metals and the ultra-fine polycrystalline metals (nc/ufc).

2.1. General descriptions of mechanics model

Referring to Fig. 1, total energy stored in material can be described as

$$\Pi = \int_V w\,dV = \sum_{i=1}^{N} \int_{V^i} w\,dV \tag{1}$$

for a bulk material or macroscopic polycrystalline material, and

$$\begin{aligned}\Pi &= \sum_{i=1}^{N} \int_{V^i} w\,dV + \sum_{j}^{M} \int_{S^j} \Gamma\,dS + \int_S \gamma\,dS \\ &= \sum_{i=1}^{N} \left\{ \int_{V^i} w\,dV + \frac{1}{2}\int_{S^i} \Gamma\,dS \right\} - \frac{1}{2}\int_S \Gamma\,dS + \int_S \gamma\,dS \\ &\approx \sum_{i=1}^{N} \left\{ \int_{V^i} w\,dV + \frac{1}{2}\int_{S^i} \Gamma\,dS \right\}\end{aligned} \tag{2}$$

for a nano- or micro-structured material when grain size is within nano- or micro-scale. In Eq. (2), material size considered is much larger than that of nano-structure, so both $\int_S \Gamma\,dS$ and $\int_{S_\gamma} \Gamma\,dS$ are much smaller than other terms and they can be neglected. w is strain energy density. Γ is interface energy density. γ is surface energy density. Both N and M are grain number and grain boundary number, respectively. V^i and S^i are the volume and surface of the ith grain. For bulk or macroscopic case, the interface energy should be much smaller than strain energy and can be neglected,

$$\int_{V^i} w\,dV \gg \frac{1}{2}\int_{S^i} \Gamma\,dS \tag{3}$$

It should be an important question that in what condition the interface energy is comparable with the strain energy in magnitude, i.e.

$$\int_{V^i} w\,dV \sim \frac{1}{2}\int_{S^i} \Gamma\,dS \tag{4}$$

The above equivalence of scalar integrations can be further expressed as

$$w \cdot V^i \sim 1/2\Gamma \cdot S^i \quad \text{or} \quad \frac{w}{1/2\Gamma} \sim \frac{S^i}{V^i} \tag{5}$$

For a typical metal material, $\sigma_Y = 200$ MPa, $E/\sigma_Y = 300$, $1/2\Gamma \sim 0.3 \sim 1.0$ N m/m^2, we have $w \sim \sigma_Y^2/2E = 10^5 \sim 10^6$ N m/ m^3, so that the above equivalence is transferred to the following magnitude of the specific interface surface,

$$\frac{w}{1/2\Gamma} \sim \frac{S^i}{V^i} \sim 10^6\ \text{m}^{-1} \tag{6}$$

Clearly, the comparison of the strain energy and interface energy depends on the magnitude of the ratio of interface surface to volume of grain. From Eq. (6), when grain size is at micron scale, interface energy is comparable to the strain energy in magnitude. When grain size is smaller than micron scale, interface energy is dominant.

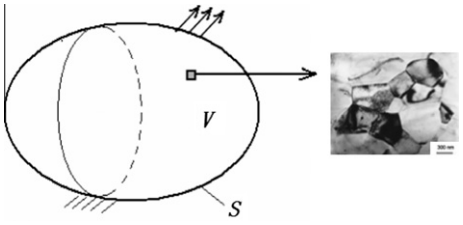

Fig. 1. Mechanics problem of nano-structured materials.

Recently, many researches have been performed to consider surface energy effect and interface energy effect based on the classical mechanics theory for homogenous materials, for example see Refs. [18,19]. For the nanocrystalline materials considering strain gradient effect without considering the interface energy effect, some researches have been done, for example see Refs. [3,20]. In order to characterize the size effects and mechanical behaviors of nanocrystalline and ultra-fine polycrystalline metals, in the present research we shall present a trans-scale mechanics model which considers both strain gradient effect and interface energy effect. The strain gradient effect is considered in total strain energy, while the interface energy effect is considered as an additional term in total potential, referring to Eq. (2).

2.2. For the case of higher-order strain gradient theory

Considering a general version of strain gradient theory [21,22] and referring to Eq. (2), the trans-scale mechanics model can be described by the following variational equation,

$$\begin{aligned}&\int_V (\sigma_{ij}\delta\varepsilon_{ij} + \tau_{ijk}\delta\eta_{ijk})dV + \delta\int_{S'} \Gamma\,dS' - \int_V f_k\delta u_k\,dV \\ &\quad - \int_S t_k\delta u_k\,dS - \int_S r_k(D\delta u_k)dS = 0\end{aligned} \tag{7}$$

Comparing with the strain gradient theory scheme (see [22]), here an additional term (the second integration term) is added, where S' is current interface area. When interface energy density Γ is considered as a material parameter, i.e. it is unchangeable with interface stress, Eq. (7) can be further simplified and written by

$$\begin{aligned}&\int_V (\sigma_{ij}\delta\varepsilon_{ij} + \tau_{ijk}\delta\eta_{ijk})dV + \int_{S^{Int}} \Gamma[R_{ij}\delta\hat{\varepsilon}_{ij} + \overline{T}_{ijpq}(\hat{\varepsilon}_{pq}\delta\tilde{\varepsilon}_{ij} + \tilde{\varepsilon}_{pq}\delta\hat{\varepsilon}_{ij})]dS \\ &\quad - \int_V f_k\delta u_k\,dV - \int_S t_k\delta u_k\,dS - \int_S r_k(D\delta u_k)dS = 0\end{aligned} \tag{8}$$

where $(\hat{\varepsilon}_{ij}, \tilde{\varepsilon}_{ij}) = (\varepsilon_{ij}^+ \pm \varepsilon_{ij}^-)/2$ are the equivalent interface strains, superscriptions "positive" and "negative" express two side values along the interface, and

$$\begin{aligned}R_{ij} &= l_i l_j + m_i m_j \\ \overline{T}_{ijpq} &= l_i l_j m_p m_q + m_i m_j l_p l_q - l_i m_j l_p m_q\end{aligned} \tag{9}$$

$(l_i, m_i)(i = 1, 3)$ are directional cosines along interface at initial configuration [23], and the unit vectors $\boldsymbol{l}$ and $\boldsymbol{m}$ are normal each other on the interface. S^{int} is interface area. From Eq. (8), the interface integration term provides the displacement derivative terms (strain components), for this kind of variational problem, a rigorous finite element method was presented, see [24]. Similarly, we can derive the similar expression with Eq. (8) for micropolar theory [25].

2.3. For the case of lower-order strain gradient theory

For a lower-order version of strain gradient theory, such as the CMSG theory (conventional theory of mechanism-based strain gradient theory) [26], variational equation can be written as

$$\int_V \sigma_{ij}\delta\varepsilon_{ij}\,dV + \int_{S^{Int}} \Gamma[R_{ij}\delta\hat{\varepsilon}_{ij} + \overline{T}_{ijpq}(\hat{\varepsilon}_{pq}\delta\hat{\varepsilon}_{ij} + \tilde{\varepsilon}_{pq}\delta\tilde{\varepsilon}_{ij})]dS - \int_V f_k\delta u_k dV - \int_S t_k\delta u_k\,dS = 0 \tag{10}$$

and written in increment form as,

$$\int_V \dot{\sigma}_{ij}\delta\dot{\varepsilon}_{ij}\,dV + \int_{S^{Int}} \Gamma\overline{T}_{ijpq}(\dot{\hat{\varepsilon}}_{pq}\delta\dot{\hat{\varepsilon}}_{ij} + \dot{\tilde{\varepsilon}}_{pq}\delta\dot{\tilde{\varepsilon}}_{ij})dS - \int_V \dot{f}_k\delta\dot{u}_k\,dV - \int_S \dot{t}_k\delta\dot{u}_k\,dS = 0 \tag{11}$$

where $(\dot{\hat{\varepsilon}}_{ij}, \dot{\tilde{\varepsilon}}) = \left(\dot{\varepsilon}^{+}_{ij} \pm \dot{\varepsilon}^{-}_{ij}\right)/2$.

Constitutive equations of the CMSG theory in increment form can be expressed as

$$\dot{\sigma}_{ij} = K\dot{\varepsilon}_{kk}\delta_{ij} + 2\mu\left\{\dot{\varepsilon}'_{ij} - \frac{3\dot{\varepsilon}}{2\sigma_e}\left[\frac{\sigma_e}{\sigma_Y\sqrt{f^2(\varepsilon^P) + l\eta^P}}\right]^m \sigma'_{ij}\right\} \tag{12}$$

where length parameter

$$l \approx 18\alpha^2\left[\frac{\mu}{\sigma_Y}\right]^2 b \tag{13}$$

is the intrinsic material length in strain gradient plasticity, σ_Y is the initial yield stress, μ is the shear modulus, b is the magnitude of the Burgers vector, α is an empirical coefficient around 0.3 depending on the material structures and characteristic, f is a non-dimensional function of plastic strain ε^p, which takes the form

$$f(\varepsilon^p) = \left(1 + \frac{E\varepsilon^P}{\sigma_Y}\right)^N \tag{14}$$

for a power-law hardening solid, E is the Young's modulus, and N is strain hardening exponent ($0 \leqslant N < 1$). About m, Huang et al. [26] demonstrated that power law visco-plastic model [27,28] incorporating the strain gradient effects can be applicable to conventional power-law hardening if the rate-sensitivity exponent m is large ($m \geqslant 20$), so in the present research, we take $m = 20$. $\dot{\varepsilon} = \sqrt{\frac{2}{3}\dot{\varepsilon}'_{ij}\dot{\varepsilon}'_{ij}}$ is the effective strain rate and $\dot{\varepsilon}'_{ij}$ is the deviatoric strain rate. K is the volume modulus of elasticity, $\sigma_e = \sqrt{3/2\sigma'_{ij}\sigma'_{ij}}$ is the Von Mises effective stress, $\dot{\varepsilon}_{kk}$ is the volume strain rate, and δ_{ij} is the Kronecker delta. The effective plastic strain gradient η^p has a definition as same as that in the higher-order MSG theory [29], and is given by

$$\eta^p = \int \dot{\eta}^p dt, \quad \dot{\eta}^p = \sqrt{\frac{1}{4}\dot{\eta}^p_{ijk}\dot{\eta}^p_{ijk}}, \quad \dot{\eta}^p_{ijk} = \dot{\varepsilon}^p_{ik,j} + \dot{\varepsilon}^p_{jk,i} - \dot{\varepsilon}^p_{ij,k}, \tag{15}$$

where $\dot{\varepsilon}^p_{ij}$ is the tensor of plastic strain rate.

Since the CMSG theory does not involve the higher-order stress, equilibrium equations and traction boundary conditions remain the same as the conventional theories. Therefore, for simplicity in the present research we shall adopt the CMSG theory in developing our computational method.

3. Computational methods

Generally speaking, when either strain gradient effects or interface energy effects are considered, the conventional finite element method fails to be used because boundary conditions include the conditions of displacement derivatives, this can be observed from Eqs. (8), (10), and (11). For this case, An effective finite element method has been presented by Wei [24], in which nodal variables are pure displacement derivatives. If the strain gradient effect is only considered and the CMSG theory is used to describe the effect, one can use the conventional displacement-based finite element method, because the lower-order theory does not involve the higher-order stresses such that the governing equations are essentially the same as those in the classical theory. When interface energy effect must be considered, the interface conditions with displacement derivatives should be presented (see Eqs. (10) or (11)). However, in the computation scheme of present research, the interface conditions will be satisfied by using another method, solution iteration.

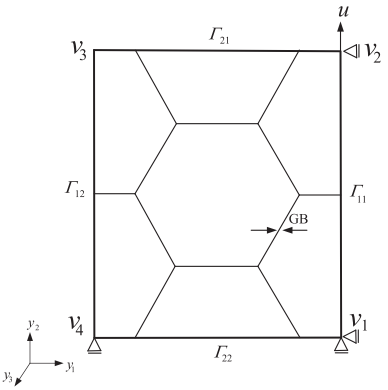

Fig. 2. A representative cell model for nano- or ultra-fine polycrystalline metal with periodic boundary conditions of y_1y_2 plane and y_3 direction.

In the present research, we shall use the CMSG theory. We can modify the existing finite element program to incorporate the plastic strain gradient effect approximately [30]. We have implemented a C^0 three-dimensional solid element incorporating the CMSG theory in the ABAQUS finite element program via its User-Material subroutine UMAT.

3.1. Finite element method (FEM) and boundary conditions

To particularly study the mechanical behaviors of the nc/ufc materials, and to investigate how the competition of grain-boundary deformation with that in the grain interiors determines the observed overall stress–strain response and the overall ductility of polycrystalline aggregates by various properties of grain boundaries and grain interiors. A regular quasi-three-dimensional representative volume element with taking into account of three dimensional effects is presented here. Fig. 2 shows the schematic drawing of representative calculation model. The calculation model is consisted of seven idealized hexagon grains, and the diameter of grain d is the diameter of circumcircle of hexagon.

As displayed in Fig. 2, periodic boundary conditions are enforced along the four sides in y_1y_2 coordinate plane [31]:

$$\bar{\mathbf{u}}_{12} - \bar{\mathbf{u}}_{v_4} = \bar{\mathbf{u}}_{11} - \bar{\mathbf{u}}_{v_1} \tag{16}$$

$$\bar{\mathbf{u}}_{22} - \bar{\mathbf{u}}_{v_1} = \bar{\mathbf{u}}_{21} - \bar{\mathbf{u}}_{v_2} \tag{17}$$

$$\bar{\mathbf{u}}_{v_3} - \bar{\mathbf{u}}_{v_2} = \bar{\mathbf{u}}_{v_4} - \bar{\mathbf{u}}_{v_1} \tag{18}$$

Here $\bar{\mathbf{u}}_{ij}$ is the displacement vector for any material point on the corresponding boundary Γ_{ij}, and $\bar{\mathbf{u}}_{v_i}$ is the displacement vector for each vertex v_i. Rigid body motions can be eliminated by requiring that $\bar{\mathbf{u}}_{v_k} = 0$, for either $k \in \{1, 2, 4\}$. Otherwise, a displacement boundary condition $\bar{\mathbf{u}}_Z$ which considers the third dimensional effect is enforced in the y_3 coordinate direction perpendicular to y_1y_2 coordinate plane, assuming that the material geometry in z direction is also a periodic structure which has a finite-thickness.

In the finite element calculation, the interface energy effect, i.e. the second integration term in Eq. (11), can be calculated through iteration: in the first step, to solve the Eq. (11) by neglecting the interface energy effect; in the second step, to solve the Eq. (11) based on the previous solution which is used to calculate the interface energy effect; and so on.

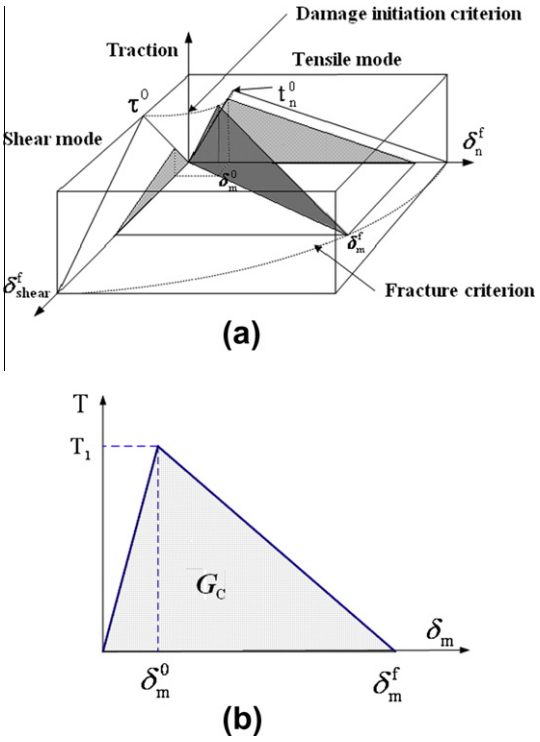

Fig. 3. (a) Illustration of mixed-mode cohesive interface model and (b) a simple total traction–separation relation.

3.2. Cohesive interface model used in describing grain boundary damage and fracture

The intergranular damage and fracture processes are described by using the cohesive interface model. Cohesive interface model was presented early in the literature Barenblatt [32] and Dugdale [33] to model fracture of solids more than 40 years ago. In recent years, numerous cohesive interface model formulations have been widely presented and used to simulate fracture initiation and propagation [34–36], and the traction–separation relations of cohesive interface are extended to represent the damage and fracture process of grain boundaries [14,15,37]. In the current numerical study, a mixed-mode cohesive interface model developed by Turon et al. [38] will be used to describe the initiation and evolution of intergranular cracks without arbitrarily introducing initial cracks. The normal and shear components of traction or displacement across the interface are combined based on a certain mixed-mode behavior. The schematic representation of the dependence of damage initiation and evolution on the mode mixes, for a traction–separation response with isotropic shear behavior is shown in Fig. 3a. The figure shows the traction on the vertical axis and the magnitudes of the normal and the shear separations along the two horizontal axes. The unshaded triangles in the two vertical coordinate planes represent the response under pure normal and pure shear deformation, respectively. All intermediate vertical planes (that contain the vertical axis) represent the damage response under mixed-mode conditions with different mode mixes. To describe the evolution of damage under a combination of normal and shear deformation across the interface, it is useful to introduce an effective displacement defined as

$$\delta_m = \sqrt{\langle \delta_n \rangle^2 + \delta_s^2 + \delta_t^2}. \tag{19}$$

where symbol $\langle\rangle$ represents the Macaulay bracket, is used to signify that a pure compressive deformation does not initiate damage. δ_n, δ_s and δ_t represent the relative displacements when the deformation is either purely normal to the interface or purely in the first or the second shear direction respectively. The mixed-mode traction–separation relations with a linear damage evolution are illustrated in Fig. 3b. Here T is traction, δ_m^0 is the critical separation effective displacement at damage initiation, T_1 corresponds to critical traction and δ_m^f is separation effective displacement at complete failure and $K_c' = T_1/\delta_m^0$ is the initial slope of linear interface separation relation, the initial separation stiffness of cohesive element, referring to Fig. 3b. Referring to Fig. 2, the separation process of grain boundary between two hexagon grains is modeled by using the cohesive interface layers with zero thickness.

4. Results and discussions

A comparative parameter study for overall strength and ductility of polycrystalline aggregates affected by the material parameters of grain boundaries and grain interiors with different grain sizes is performed. The overall stress–strain relation of the nanostructured materials with parameter dependence normalized by the initial yield stress σ_y and intrinsic material length l as well as grain size d can be expressed as follows

$$\frac{\sigma}{\sigma_y} = F\left(\varepsilon; \frac{E}{\sigma_y}, \nu, N, \frac{d}{l}, \frac{\Gamma}{\sigma_y d}, \frac{T}{\sigma_y}, \frac{K_c}{\sigma_y}, \frac{\delta_m^f - \delta_m^0}{l}\right) \tag{20}$$

where the intragranular material parameters are Young's modulus E, Poisson's ratio ν, initial yield stress σ_y, strain hardening exponent N, respectively. The interfacial parameters of grain boundary are interface energy density Γ, separation traction T, effective initial separation modulus $K_c = K_c' l = T_1/(\delta_m^0/l)$, and the effective damage evolution displacement $\left(\delta_m^f - \delta_m^0\right)$. The geometrical parameter is the grain size d. In the analysis of present paper, we take K_c value as Young's modulus of crystal grain for no influence on solution feature, referring to $\sigma_Y/E \sim 0.6\%$ for most alloys.

Fig. 4 shows the dependence of the overall stress–strain relations on the intragranular strain hardening exponent N for different grain sizes $d = 0.1l$ and $d = l$ and different interface energy densities $\alpha_\Gamma = \Gamma/\sigma_y d = 0.01$ and 1.0. In the analysis, we take $N = 0.1$ and 0.2, respectively. From Fig. 4, the overall ductility of nanocrystalline materials are sensitive to strain hardening exponent N, while the overall strength of the nanocrystalline materials are not sensitive to the parameter N. There exists an obvious difference on ductility for $N = 0.1$ and 0.2. The effect of composite parameter, $\alpha_\Gamma = \Gamma/\sigma_y d$, of the either interface energy density or grain size, is obvious. In Fig. 4, the maximum separation strength T_1 and the cohesive zone energy density G_c keep unchangeable,

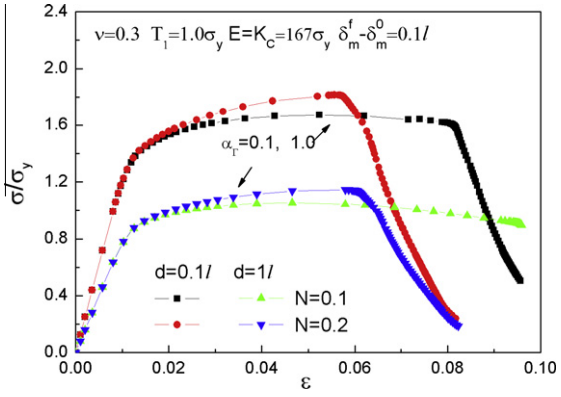

Fig. 4. Dependence of overall stress–strain curves on strain hardening exponent (N) of grain material and grain size and interface energy density ($\alpha_\Gamma = \Gamma/\sigma_y d$).

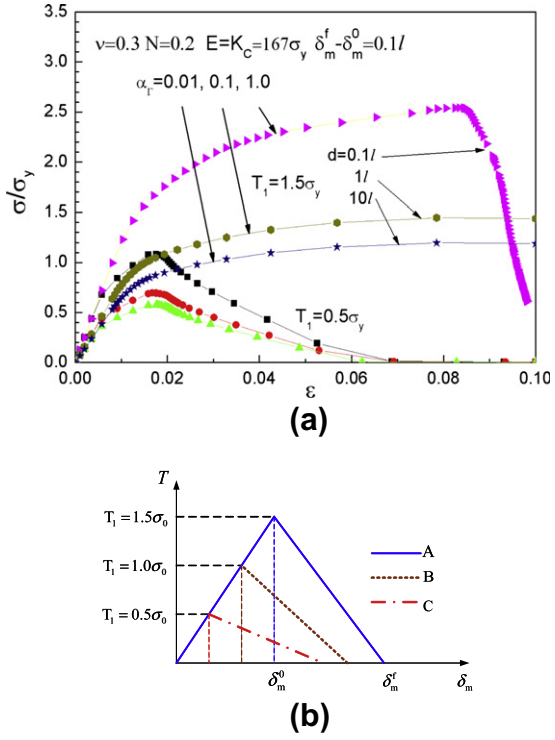

Fig. 5. Dependence of overall stress–strain curves on separation strength (T_1/σ_y) and grain sizes (d/l) and interface energy density ($\alpha_\Gamma = \Gamma/\sigma_y d$).

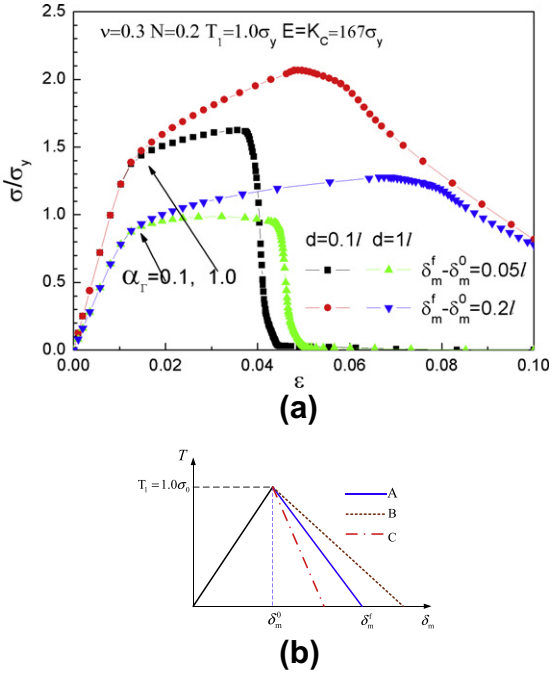

Fig. 6. Overall stress–strain curves related to the cohesive zone ductility $\left(\delta_m^f - \delta_m^0\right)$ and grain sizes (d/l) as well as the interface energy density ($\alpha_\Gamma = \Gamma/\sigma_y d$).

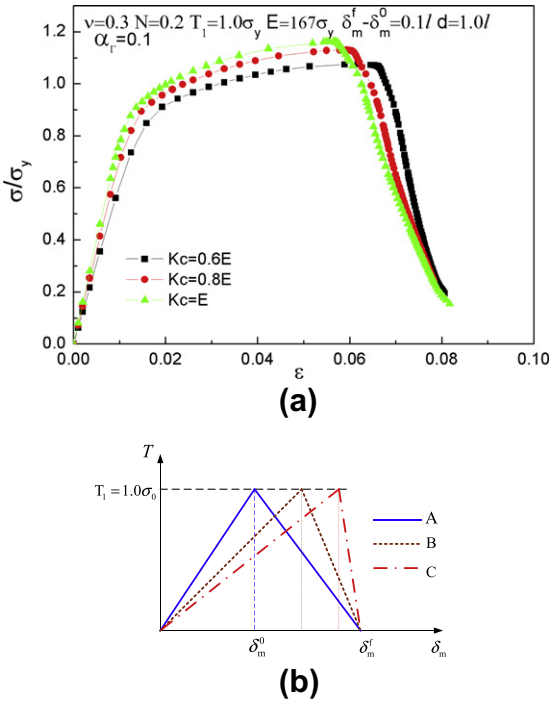

Fig. 7. Overall stress–strain curves relate to the effective elastic modulus of cohesive relation (K_C), keeping other effects unchangeable.

and the differences among overall stress–strain curves are come from material parameters, interface energy density and grain size.

Fig. 5a shows the dependence of overall stress–strain relations on the maximum separation strength T_1/σ_y, composite parameter $\alpha_\Gamma = \Gamma/\sigma_y d$, as well as the grain sizes ($d = 0.1l$, l and $10l$). For results in this figure, we consider two cases of $T_1/\sigma_y = 0.5$ and 1.5, for $\alpha_\Gamma = \Gamma/\sigma_y d = 0.01$, 0.1 and 1.0, respectively. The results show that the overall strength and ductility of nanocrystalline materials are very sensitive to the ratio T_1/σ_y and the dimensionless parameter $\alpha_\Gamma = \Gamma/\sigma_y d$. The tensile strength and ductility of nanocrystalline materials increase greatly for the ratio $T_1/\sigma_y = 1.5$ respect to $T_1/\sigma_y = 0.5$. The grain size effects or interface energy effects in inelastic deformation are much big with increasing the value of T_1/σ_y. Furthermore, for grain diameter $d \geqslant l$, the dependence of intergranular fracture on the grain size is gradually diminished. For $d/l = 0.1$, the grain size effects in plastic flow are much big. From Fig. 5a, both T_1/σ_y and $\alpha_\Gamma = \Gamma/\sigma_y d$ are the critical control parameters for the competition of grain-boundary deformation with that in the grain interiors to define the global strength and ductility of nano-structured materials. The intragranular elastic–plastic deformation would be dominant and the nano- or polycrystalline materials display good ductility and high strength when $T_1 \geqslant \sigma_y$ and $\alpha_\Gamma = \Gamma/\sigma_y d > 0.1$. Otherwise the grain boundaries related slip and separation phenomena maybe begun to play an important role in the overall inelastic response of nano- or polycrystalline materials and a brittle fracture would be appearance for $T_1 < \sigma_y$ and $\alpha_\Gamma = \Gamma/\sigma_y d < 0.1$. In the nc/ufc metals, the dislocation-based slip processes in the grain interiors are restrained gradually while the intragranular initial yield stresses are getting higher with decreasing grain sizes. So improving the resistance of grain boundaries to intergranular fracture may be an effective method to improve the bulk properties.

In Fig. 5a, two sets of the maximum separation strength T_1 and the cohesive energy density G_c are considered, see the case A and case C in Fig. 5b, which correspond to two sets of results and compare with each other. The case A corresponds to larger values of T_1 and G_c, while case C corresponds to smaller values of them. From the results shown in Fig. 5a, both T_1 and G_c are dominant parameters at interface. On the other hand, from Fig. 5a, additional dominant parameter is the interface energy density at nanoscale.

Fig. 6a shows how the variation of damage evolution range $\left(\delta_m^f - \delta_m^0\right)$ of cohesive interfacial model influences the overall

stress–strain relations for two grain size (d) values and for two composite parameter (α_Γ) values. From Fig. 6a, both the ductility and strength of materials undergo an obvious increase, specifically, the ductility undergoes a huge increase with increase in damage evolution range. In this case, the composite parameter α_Γ is also a dominant parameter.

In the results shown in Fig. 6a, we keep the maximum separation strength T_1 to be unchangeable, and increase G_c by increasing $\delta_m^f - \delta_m^0$, see Fig. 6b. Obviously, the ductility of materials is very sensitive to G_c value increase.

In Fig. 7a, the overall stress–strain relations are shown for the cases when T_1, G_c, as well as α_Γ values keep unchangeable (see Fig. 7b). From Fig. 7a, very small differences among the computational results for different elastic slopes of cohesive model are observed. These further delineate that there exist three and only three parameters which are important interface parameters.

5. Conclusion remarks

A trans-scale mechanics model for describing the mechanical behavior and size effect for nanostructured materials has been developed in the present research. For the mechanics model, both strain gradient effect and interface energy effect are considered. Based on the trans-scale mechanics model, a finite element method has been developed, which considers not only the trans-scale characteristics of materials, but also the damage and fracture processes by using the cohesive zone model. By using the above theoretical and computational model, we have displayed the overall stress–strain relations for the nc/ufc materials systematically, and we have also displayed the micro-scale plastic deformation characteristics in polycrystalline aggregates with nc/ufc grains. Through the systematical studies on the overall strength and ductility of polycrystalline aggregates, we conclude that the overall strength and ductility of polycrystalline aggregates with nc/ufc grains have been dominated by four important parameters, (α_Γ, T_1, G_c, N), in which $\alpha_\Gamma = \Gamma/\sigma_y d$ relates either the interface energy density or grain size, N is strain hardening exponent, and other two parameters relate to the interface adhesion strength, ductility and damage.

It is worth noting that in the present research, several assumptions and simplifications are adopted, which should cause the deviation between modeling results and experimental measurements. Firstly, the calculation model is a quasi-three-dimensional cell model and is assumed periodic structures in both y_1y_2 plane and normal direction (z direction). Secondly, the distributions of the real grain sizes are very complicated, while in the present calculation model the distributions are assumed regularly. Thirdly, in the present model, the selections of the input parameters for the grain boundary cohesive model and interiors are difficult to be defined correctly due to lacking of experimental data. Moreover, in order to further understand the grain boundary fracture behaviors which are usually characterized by the cohesive zone model, more efforts are still needed.

Acknowledgement

The subject is supported by the National Science Foundation of China through Grant Nos. 11021262, 10932011, and 90816004.

References

[1] H. Gleiter, Acta Mater. 48 (2000) 1.
[2] K.S. Kumar, H. Van Swygenhoven, S. Suresh, Acta Mater. 51 (2003) 5743.
[3] Y.G. Wei, S. Shu, Y. Du, C. Zhu, Int. J. Plast. 21 (2005) 2089.
[4] Zhiwei Shan, E.A. Stach, J.M.K. Wiezorek, J.A. Knapp, D.M. Follstaedt, S.X. Mao, Science 305 (2004) 654.
[5] H. Van Swygenhoven, P.M. Derlet, Phys. Rev. B 64 (2001) 224105.
[6] A. Hasnaoui, H. Van Swygenhoven, P.M. Derlet, Science 300 (2003) 1550.
[7] J. Schiotz, T. Vegge, D. Di Tolla, K. Jacobsen, Phys. Rev. B 60 (1999) 971.
[8] K.J. Von Vliet, S. Tsikata, S. Suresh, Appl. Phys. Lett. 83 (2003) 1441.
[9] A. Cao, Y.G. Wei, Phys. Rev. B 76 (2007) 024113.
[10] Y. Wei, X. Wang, M. Zhao, J. Mater. Res. 19 (2004) 208.
[11] H.-H. Fu, D. Benson, M.A. Meyers, Acta Mater. 52 (2004) 4413.
[12] R. Schwaiger, B. Moser, M. Dao, N. Chollacoop, S. Suresh, Acta Mater. 51 (2003) 5159.
[13] Y. Wei, X. Chen, S. Shu, C. Zhu, C. Int. J. Mult. Comp. Eng. 4 (2006) 183.
[14] Y.J. Wei, L. Anand, J. Mech. Phys. Solids 52 (2004) 2587.
[15] D.H. Warner, F. Sansoz, J.F. Molinari, Int. J. Plast. 22 (2006) 754.
[16] I.A. Ovid'ko, J. Mater. Sci. 42 (2007) 1694.
[17] S. Ranganathan, R. Divakar, V.S. Ragunathan, Scripta Mater. 44 (2001) 1169.
[18] W. Gao, S.W. Yu, G.Y. Huang, Nanotechnology 17 (2006) 1118–1122.
[19] J. Wang, H.L. Duan, Z.P. Huang, B.L. Karihaloo, Proc. Roy. Soc. A 462 (2006) 1355–1363.
[20] B. Wu, Y.G. Wei, Mater. Sci. Forum 633–634 (2010) 39–53.
[21] N.A. Fleck, J.W. Hutchinson, Adv. Appl. Mech. 33 (1997) 295–361.
[22] Y. Wei, J.W. Hutchinson, J. Mech. Phys. Solids 45 (1997) 1253.
[23] X.L. Chen, H.S. Ma, L.H. Liang, Y.G. Wei, Comput. Mater. Sci. 46 (2009) 723–727.
[24] Y.G. Wei, Eur. J. Mech. A/Solids 25 (2006) 897.
[25] X.N. Liu, G.K. Hu, Int. J. Plast. 21 (2005) 777–799.
[26] Y. Huang, S. Qu, K.C. Hwang, M. Li, H. Gao, Int. J. Plast. 20 (2004) 753.
[27] J.W. Hutchinson, Proc. Roy. Soc. Lond. A 348 (1976) 101.
[28] S. Kok, A.J. Beaudoin, D.A. Tortorelli, Int. J. Plast. 18 (2002) 715.
[29] H. Gao, Y. Huang, W.D. Nix, J. Mech. Phys. Solids 47 (1999) 1239.
[30] S. Qu, Y. Huang, H. Jiang, C. Liu, P.D. Wu, K.C. Hwang, Int. J. Fract. 129 (2004) 199.
[31] O. Van der Sluis, P.J.G. Schreurs, H.E.H. Meijer, Mech. Mater. 33 (2001) 499.
[32] G.I. Barenblatt, Appl. Math. Mech. (PMM) 23 (1959) 622.
[33] D.S. Dugdale, J. Mech. Phys. Solids 8 (1960) 100.
[34] A. Needleman, J. Mech. Phys. Solids 38 (1990) 289.
[35] V. Tvergaard, J.W. Hutchinson, J. Mech. Phys. Solids 40 (1992) 1377.
[36] Y. Wei, J.W. Hutchinson, J. Mech. Phys. Solids 45 (1997) 1137.
[37] E. Iesulauro, A.R. Ingraffea, S. Arwade, P.A. Wawrzynek, Fatigue Fract. Mech. 33 (2002) 1417.
[38] A. Turon, P. Camanho, J. Costa, C. Davila, NASA/TM-2004-213277.